

SLABL<sub>U</sub>: A TWO-LEVEL SPARSE DIRECT SOLVER FOR ELLIPTIC PDES

Anna Yesypenko\* and Per-Gunnar Martinsson†

**Abstract:** The paper describes a sparse direct solver for the linear systems that arise from the discretization of an elliptic PDE on a two dimensional domain. The scheme decomposes the domain into thin subdomains, or “slabs” and uses a two-level approach that is designed with parallelization in mind. The scheme takes advantage of  $\mathcal{H}^2$ -matrix structure emerging during factorization and utilizes randomized algorithms to efficiently recover this structure. As opposed to multi-level nested dissection schemes that incorporate the use of  $\mathcal{H}$  or  $\mathcal{H}^2$  matrices for a hierarchy of front sizes, SlabLU is a two-level scheme which only uses  $\mathcal{H}^2$ -matrix algebra for fronts of roughly the same size. The simplicity allows the scheme to be easily tuned for performance on modern architectures and GPUs.

The solver described is compatible with a range of different local discretizations, and numerical experiments demonstrate its performance for regular discretizations of rectangular and curved geometries. The technique becomes particularly efficient when combined with very high-order accurate multi-domain spectral collocation schemes. With this discretization, a Helmholtz problem on a domain of size  $1000\lambda \times 1000\lambda$  (for which  $N = 100M$ ) is solved in 15 minutes to 6 correct digits on a high-powered desktop with GPU acceleration.

**Keywords:** direct solver, sparse direct solver, randomized linear algebra, multifrontal solver, high order discretization, GPU, Helmholtz equation.

## 1. INTRODUCTION

1.1. **Problem setup.** We present a direct solver for boundary value problem of the form

$$(1) \quad \begin{cases} \mathcal{A}u(x) = f(x), & x \in \Omega, \\ u(x) = g(x), & x \in \partial\Omega, \end{cases}$$

where  $\mathcal{A}$  is a second order elliptic differential operator, and  $\Omega$  is a domain in two dimensions with boundary  $\partial\Omega$ . The method works for a broad range of constant and variable coefficient differential operators, but is particularly competitive for problems with highly oscillatory solutions that are difficult to pre-condition. For the sake of concreteness, we will focus on the case where  $\mathcal{A}$  is a variable coefficient Helmholtz operator

$$(2) \quad \mathcal{A}u(x) = -\Delta u(x) - \kappa^2 b(x)u(x),$$

where  $\kappa$  is a reference (“typical”) wavenumber, and where  $b(x)$  is a smooth non-negative function. Upon discretizing (1), one obtains a linear system

$$(3) \quad \mathbf{A}\mathbf{u} = \mathbf{f},$$

involving a coefficient matrix  $\mathbf{A}$  that is typically sparse. Our focus is on efficient algorithms for directly building an invertible factorization of the matrix  $\mathbf{A}$ . We specifically consider two different discretization schemes, first a basic finite difference scheme with second order convergence, and then a high (say  $p = 20$ ) order multidomain spectral collocation scheme [52, Ch. 25]. However, the techniques presented can easily be used with other (local) discretization schemes such as finite element methods.

\*Oden Institute, University of Texas at Austin. Email: annayes@utexas.edu

†Oden Institute, University of Texas at Austin. Email: pgm@oden.utexas.edu

**1.2. Overview of proposed solver.** The solver presented is based on a decomposition of the computational domain into thin “slabs”, as illustrated in Figure 1a. Unlike previously proposed sweeping schemes [22,32,61] designed for preconditioning, our objective is to directly factorize the coefficient matrix, or at least compute a factorization that is sufficiently accurate that it can handle problems involving strong backscattering.

To describe how the solver works, let us consider a simple model problem where the PDE is discretized using a standard five-point finite difference stencil on a uniform grid such as the one shown in Figure 1a. The nodes in the grid are arranged into slabs of width  $b$ , and are ordered as shown in Figure 1a, resulting in a coefficient matrix  $\mathbf{A}$  with the block diagonal sparsity pattern shown in Figure 1c. The factorization of  $\mathbf{A}$  then proceeds through two stages.

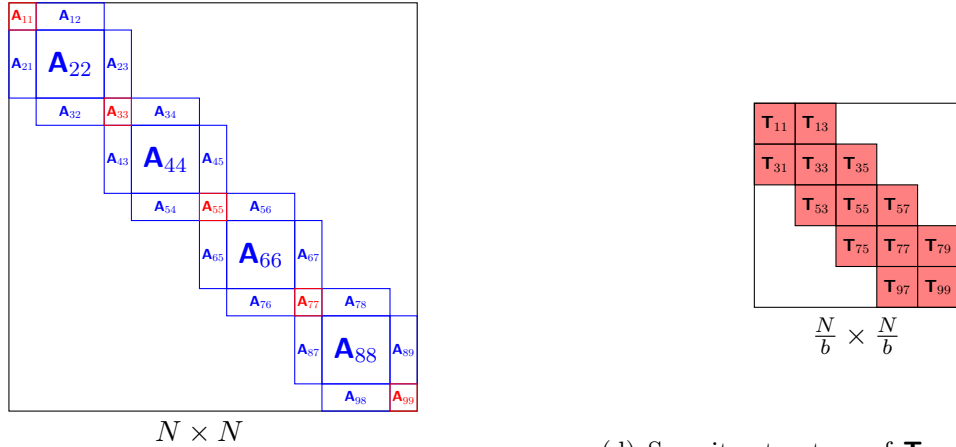
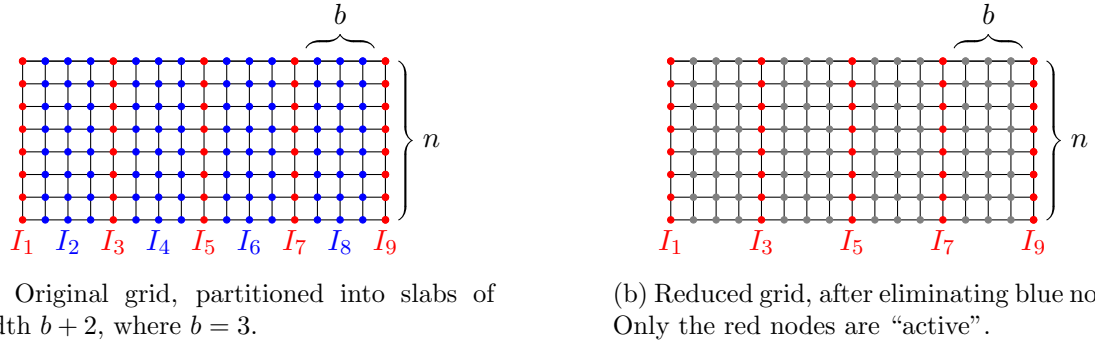


FIGURE 1. Illustration of the elimination order used in SlabLU.

In the first stage, the nodes that are internal to each slab (identified by the index vectors  $I_2, I_4, \dots$  and shown as blue in Figure 1a) are eliminated from the linear system, resulting in the reduced problem shown in Figure 1b, with the associated coefficient matrix shown in Figure 1d. In this elimination step, we exploit that each subdomain is thin, which means that classical sparse direct solvers are particularly fast. To further accelerate this step, we use that the Schur complements that arise upon the elimination of the interior nodes are rank structured. Specifically, they are “HBS/HSS matrices” [41, 64, 65] with *exact* HBS/HSS rank at most  $2b$ . This allows us to accelerate this reduction step using a recently proposed randomized algorithm for compressing rank structured matrices [46].

The second stage is to factorize the remaining coefficient matrix  $\mathbf{T}$  shown in Figure 1d. This matrix is much smaller than the original matrix  $\mathbf{A}$ , but the sub-blocks are dense. Because we have efficiently formed  $\mathbf{T}$  with  $\mathcal{H}^2$ -matrix structure, the reduced system can be factorized in linear time for many elliptic PDEs (e.g. any coercive elliptic PDE, the steady state Stokes equation, and Helmholtz in the regime that the wavenumber is fixed as  $N$  grows). With the use of  $\mathcal{H}^2$ -matrix algebra to factorize  $\mathbf{T}$ , SlabLU requires linear time to store and factorize when the slab widths are chosen to be  $\mathcal{O}(1)$ . In this work, we choose the slab width  $b$  to grow slowly with the discretization size  $N$  for performance considerations.

Our two-level framework offers a distinct advantage in terms of simplicity in both implementation and optimization. In the first stage, we can leverage existing sparse direct solvers, which prove to be highly efficient, especially for thin 2D slabs. As we progress to the second stage, the fronts become larger in size, which may present a challenge when using traditional techniques. The key benefit of SlabLU, in contrast to multi-level schemes, lies in the fact that we only need to develop specialized linear algebraic techniques for fronts of approximately the same size in the second stage. This stands in contrast to the necessity of developing such techniques for a hierarchy of front sizes in multi-level schemes.

We have found that for 2D problems, the dense operations are fast enough that exploiting rank structure to factorize  $\mathbf{T}$  is not worthwhile when  $N \leq 10^8$ . Specifically, by choosing  $b \sim \mathcal{O}(\sqrt{n})$ , sparsity alone results in complexity  $\mathcal{O}(N^{1.75})$  for the factorization stage, and  $\mathcal{O}(N^{1.25})$  for the solve stage, when applied to 2D problems. The simplicity of the two-level scheme allowed for parts of the factorization to be offloaded and accelerated on the GPU. For meshes with 100 million points, the factorization can be computed in 20 minutes on a desktop with an Intel i9-12900k CPU with 16 cores and an RTX 3090 GPU. Once the factorization is available, subsequent solves take about a minute. The numerical results feature timing results on a variety of architectures to demonstrate that the scheme is portable to many hardware settings.

The scheme also interacts very well with high order discretization schemes such as those described in [55] and [52, Ch. 25], which makes it a particularly powerful tool for solving problems with highly oscillatory solutions. The numerical results feature constant and variable coefficient Helmholtz problems on rectangular and curved domains. Using high order discretizations, we are able to discretize the PDE to 10 points per wavelength and accurately resolve solutions on domains of size  $1000\lambda \times 1000\lambda$ , where  $\lambda$  is the wavelength, to 6 digits of relative accuracy, compared to the true solution of the PDE.

**1.3. Context and related work.** Methods to solve (3) can be characterized into two groups – direct and iterative. The linear systems involved are typically ill-conditioned, which necessitates the use of specialized solvers. For problems with non-oscillatory solutions, multigrid methods are often highly effective [15, 60, 67]. For oscillatory problems, multigrid works less well [27]. Specialized preconditioners have been developed, and work well for many classes of problems, in particular those involving free-space problems [25, 26, 31, 33]. In this context, the sweeping preconditioners of Engquist and Ying are of particular relevance, as they were an inspiration for the current work [22, 23]. However, oscillatory problems remain highly challenging to pre-condition, in particular in situations involving strong back-scattering, cavities, or problems trapped inside a finite domain. Sparse direct methods, which factorize the matrix  $\mathbf{A}$  exactly, offer a robust means of solving challenging PDEs. They are also particularly advantageous in situations involving multiple right-hand sides or low-rank updates to the matrix  $\mathbf{A}$ .

The solver we describe in this work is related to multi-frontal LU solvers [19] which often use a hierarchical nested dissection ordering of grid nodes [4, 35]. For a 2D grid with  $N$  nodes, the resulting techniques have complexity  $\mathcal{O}(N^{3/2})$  to build and  $\mathcal{O}(N \log N)$  complexity

to solve, which is known to be work optimal among solvers that exploit only sparsity in the system [18, 21]. The  $\mathcal{H}$  and  $\mathcal{H}^2$ -matrix algebras can be used to reduce the complexity of operations on dense matrices that arise in many contexts involving the discretization of integral equations and of PDEs [10, 14, 42]. SlabLU is inspired by prior work in sparse direct solvers for PDEs which uses  $\mathcal{H}$ -matrices [3, 16, 36, 40, 59, 66]. In particular, we were inspired by [16] which used a domain partitioning into planes (e.g.  $b = 1$ ) for a highly effective linear solver for low order discretizations.

A key feature of SlabLU is that unlike prior work, the rank structures that we exploit are *exact*, relying only on the sparsity pattern of the original coefficient matrix (cf. Section 3.2). This makes the randomized compression particularly efficient, achieving very high computational efficiency with no loss of accuracy beyond floating point errors. Another novelty is the usage of a recently developed black box randomized algorithm for compressing rank structured matrices [45] (which in turn draws on insights from [49, 51, 54]) when eliminating the interior nodes in each slab.

Importantly, the rank-deficiencies used for thin subdomains in SlabLU are present in both the non-oscillatory and oscillatory regimes. Similar observations are used to develop efficient solvers for integral equation discretizations on elongated domains [56, 57]. In the general case, the interaction rank grows algebraically with the wavenumber [24], making the efficient use of  $\mathcal{H}$  and  $\mathcal{H}^2$  matrix techniques challenging, though it has been observed to work well in some situations [8, 12, 63]. For the purposes of this work which focuses on 2D domains, we only use  $\mathcal{H}^2$ -matrix compression to form the reduced system  $\mathbf{T}$  efficiently, then use highly efficient dense linear algebra routines to factorize the reduced system, an approach which we demonstrate to be effective in the numerical results section.

**1.4. Extensions and limitations.** The solver presented is purely algebraic and can be applied to a range of different discretization schemes, including finite element and finite volume methods. In this manuscript, we restrict attention to regular discretizations of domains that are either rectangular themselves, or can be mapped smoothly to a union of elongated rectangles or slabs. It is possible to adapt the method to more general discretizations with local refinement, so long as it is simple to partition the computational domain into index sets corresponding to elongated slabs. For some high order discretizations (e.g. high order finite differences), widening stencils may lead to large pre-factors when using SlabLU, though this is also a challenge for sparse direct solvers in general [52, Ch. 20].

While we in this manuscript restrict attention to the two dimensional case, the method is designed to handle three dimensional problems as well. All ideas presented carry over directly, but additional complications do arise. The key challenge is that in three dimensions, it is no longer feasible to use dense linear algebra when factorizing the block tridiagonal reduced coefficient matrix  $\mathbf{T}$ . However, the 3D version of SlabLU is also very easy to parallelize, and the idea of using randomized compression combined with efficient sparse direct solvers to eliminate the nodes interior to each slab still applies, cf. Section 7.

## 2. DISCRETIZATION AND NODE ORDERING

We introduce two different discretization techniques for (1). The first is simply the standard second order accurate five point finite difference stencil. Since this discretization is very well known, it allows us to describe how the solver works without the need to introduce cumbersome background material. To demonstrate that the solver works for a broader class of discretization schemes, the numerical experiments reported in Section 6 also include results that rely on the high order accurate *Hierarchical Poincaré-Steklov (HPS)* scheme, which we briefly describe in Section 2.3.

**2.1. A model problem based on the five point stencil.** For purposes of describing the factorization scheme, let us introduce a very simple discretization of the boundary value problem (1). We work with a rectangular domain  $\Omega = [0, L_1] \times [0, L_2]$  and the second order linear elliptic operator  $\mathcal{A}$  defined by (2). We assume that  $L_1 \geq L_2$ , and that  $L_1 = hn_1$  and  $L_2 = hn_2$  for some grid spacing  $h$  and some positive integers  $n_1$  and  $n_2$ . We then discretize  $\mathcal{A}$  with a standard second-order finite difference scheme, to obtain the linear system

$$(4) \quad \frac{1}{h^2} (\mathbf{u}(n_w) + \mathbf{u}(n_e) + \mathbf{u}(n_n) + \mathbf{u}(n_s) - 4\mathbf{u}(n)) - \kappa^2 \mathbf{b}(n) \mathbf{u}(n) = \mathbf{f}(n).$$

The vector  $\mathbf{f}$  holds values of the body load at the discretization nodes, and the vector  $\mathbf{u}$  holds approximations to the solution  $u$ . See Figure 2 for a visualization of the 5 point stencil. We write the system (4) compactly as  $\mathbf{A}\mathbf{u} = \mathbf{f}$ .

**2.2. Clustering of the nodes.** We next subdivide the computational domain into thin “slabs”, as shown in Figure 1a. We let  $b$  denote the number of grid points in each slab ( $b = 4$  in Figure 1a), and then introduce index vectors  $I_1, I_2, I_3, \dots$  that keep track of which slabs each grid point belongs to. The odd numbered index vectors  $I_1, I_3, I_5, \dots$  indicate nodes on the interfaces between slabs (red in Figure 1a), while the even numbered ones indicate nodes that are interior to each slab (blue in Figure 1a). With this ordering of the grid points, the stiffness matrix associated with the discretization (4) has the sparsity pattern shown in Figure 1c.

**2.3. High order discretizations.** To accurately resolve oscillatory wave phenomena, we rely on a high order accurate multi-domain spectral collocation discretization known as the Hierarchical Poincaré-Steklov scheme (HPS). This discretization scheme is designed to allow for high choices of the local discretization order  $p$  without degrading the performance of direct solvers. In HPS, the computational domain is subdivided into small subdomain, and a  $p \times p$  tensor product grid of Chebyshev nodes is placed on each subdomain.

As a brief illustration of the discretization scheme, consider a partitioning of  $\Omega$  into two subdomain, cf. Figure 3. For the nodes internal to each subdomain, we discretize (3) through collocation of the spectral differentiation operator. For the nodes on boundaries between subdomains, we enforce continuity of the normal derivatives.

To improve efficiency when HPS is combined with sparse direct solvers, we “eliminate” the nodes internal to each subdomain by partially computing an LU decomposition for the internal nodes that decouples them from the rest of system. This process is known as static condensation and leads a reduced system

$$(5) \quad \tilde{\mathbf{A}}\tilde{\mathbf{u}} = \tilde{\mathbf{f}}$$

with modified interactions between subdomain interfaces. The discretization can be generalized to any domain that can be smoothly mapped to a union of square subdomains, cf. Figure 4. For further details, see [52, Ch. 25], as well as [7, 9, 34, 39, 43, 55].

Because spectral differentiation is a dense operator, static condensation requires  $\mathcal{O}(p^4 N)$  flops and the solution operators for each subdomain require  $\mathcal{O}(p^2 N)$  bits to store. In our implementation, we use the fact that the leaf operations can be done in parallel and attain high performance on the GPU with batched linear algebra, which we demonstrate to be an effective approach for  $p$  up to 42 in [69]. The leaf operations are so efficient that we discard the factorized operators on leaf nodes to save on space and refactorize as needed, cf. Section 5.3.

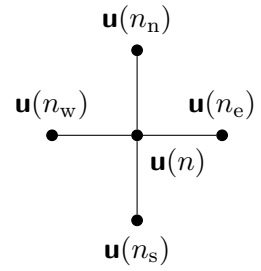


FIGURE 2. Five-point stencil in 2D.

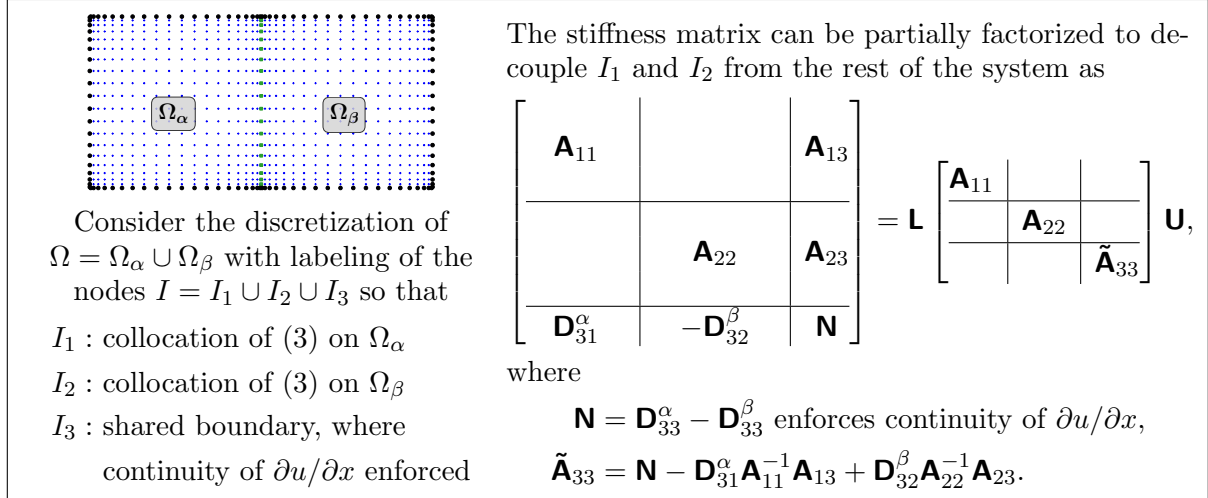


FIGURE 3. The figure above provides an illustration of static condensation for a simple HPS discretization of two subdomains for (3) with Dirichlet data prescribed. See [52, Ch. 24] for further details on the details of the discretization. Static condensation is the process of partially factorizing  $\mathbf{A}$  and decoupling the nodes internal to each subdomain from the rest of the system. The reduced system (5) is on the interfaces between subdomains.

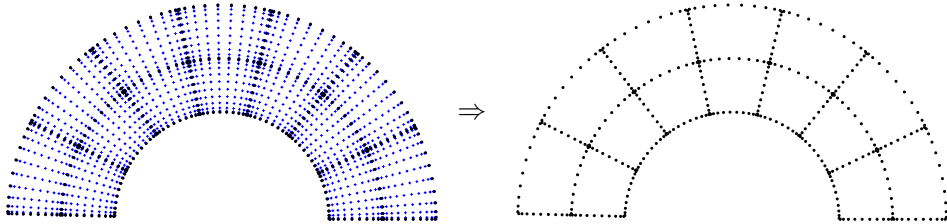


FIGURE 4. HPS is a multi-domain spectral collocation scheme where the PDE is enforced on each subdomain interior using dense spectral differentiation. Prior to interfacing with SlabLU, we “eliminate” the interior blue nodes in parallel and produce an equivalent system to solve on the boundaries. The original grid has  $n_1 \times n_2$  points, and remaining grid has  $\approx n_1 n_2 / p$  points.

For efficiently handling higher orders of  $p$ , one can use ultraspherical polynomials [58] instead of Chebyshev polynomials which lead to sparse and well-conditioned differentiation on the leaf nodes, see [6, 29, 30] for efficient multi-domain spectral methods on 2D volumes and [28] for methods on surface PDEs.

**Remark 1.** *A key point of the present work is that the solver has only two levels, which makes the “H” in “HPS” a slight misnomer, as it refers to “hierarchical”. We nevertheless stick with the “HPS” acronym to conform with the prior literature.*

### 3. STAGE ONE: ELIMINATION OF NODES INTERIOR TO EACH SLAB

This section describes the process that we use to eliminate the nodes interior to each slab that we sketched out in Section 1.2. The objective is to reduce the sparse stiffness matrix  $\mathbf{A}$  (illustrated in Figure 1c) into the smaller block tridiagonal matrix  $\mathbf{T}$  (illustrated in Figure 1d). The techniques described form the core algorithmic innovation of the manuscript.

**3.1. Schur complements.** With the ordering introduced in Section 2.2, the coefficient matrix  $\mathbf{A}$  has the block form

$$(6) \quad \begin{bmatrix} \mathbf{A}_{11} & \mathbf{A}_{12} & \mathbf{0} & \mathbf{0} & \mathbf{0} & \dots \\ \mathbf{A}_{21} & \mathbf{A}_{22} & \mathbf{A}_{23} & \mathbf{0} & \mathbf{0} & \dots \\ \mathbf{0} & \mathbf{A}_{32} & \mathbf{A}_{33} & \mathbf{A}_{34} & \mathbf{0} & \dots \\ \mathbf{0} & \mathbf{0} & \mathbf{A}_{43} & \mathbf{A}_{44} & \mathbf{A}_{45} & \dots \\ \vdots & \vdots & \vdots & \vdots & \vdots & \vdots \end{bmatrix} \begin{bmatrix} \mathbf{u}_1 \\ \mathbf{u}_2 \\ \mathbf{u}_3 \\ \mathbf{u}_4 \\ \vdots \end{bmatrix} = \begin{bmatrix} \mathbf{f}_1 \\ \mathbf{f}_2 \\ \mathbf{f}_3 \\ \mathbf{f}_4 \\ \vdots \end{bmatrix}.$$

We eliminate the vectors  $\mathbf{u}_2, \mathbf{u}_4, \mathbf{u}_6, \dots$  that represent unknown variables in the interior of each slab through a step of block Gaussian elimination. To be precise, we insert the relation

$$(7) \quad \mathbf{u}_i = \mathbf{A}_{ii}^{-1}(\mathbf{f}_i - \mathbf{A}_{i,i-1}\mathbf{u}_{i-1} - \mathbf{A}_{i,i+1}\mathbf{u}_{i+1}), \quad i = 2, 4, 6, \dots$$

into the odd-numbered rows in (6) to obtain the reduced system

$$(8) \quad \begin{bmatrix} \mathbf{T}_{11} & \mathbf{T}_{13} & \mathbf{0} & \mathbf{0} & \mathbf{0} & \dots \\ \mathbf{T}_{31} & \mathbf{T}_{33} & \mathbf{T}_{35} & \mathbf{0} & \mathbf{0} & \dots \\ \mathbf{0} & \mathbf{T}_{53} & \mathbf{T}_{55} & \mathbf{T}_{57} & \mathbf{0} & \dots \\ \mathbf{0} & \mathbf{0} & \mathbf{T}_{57} & \mathbf{T}_{77} & \mathbf{T}_{79} & \dots \\ \vdots & \vdots & \vdots & \vdots & \vdots & \vdots \end{bmatrix} \begin{bmatrix} \mathbf{u}_1 \\ \mathbf{u}_3 \\ \mathbf{u}_5 \\ \mathbf{u}_7 \\ \vdots \end{bmatrix} = \begin{bmatrix} \tilde{\mathbf{f}}_1 \\ \tilde{\mathbf{f}}_3 \\ \tilde{\mathbf{f}}_5 \\ \tilde{\mathbf{f}}_7 \\ \vdots \end{bmatrix},$$

where the sub-blocks of  $\mathbf{T}$  are defined as

$$(9) \quad \mathbf{T}_{11} = \mathbf{A}_{11} - \mathbf{A}_{12} \mathbf{A}_{22}^{-1} \mathbf{A}_{21},$$

$$(10) \quad \mathbf{T}_{13} = \mathbf{A}_{13} - \mathbf{A}_{12} \mathbf{A}_{22}^{-1} \mathbf{A}_{23},$$

$$(11) \quad \mathbf{T}_{31} = \mathbf{A}_{31} - \mathbf{A}_{32} \mathbf{A}_{22}^{-1} \mathbf{A}_{23},$$

$$(12) \quad \mathbf{T}_{33} = \mathbf{A}_{33} - \mathbf{A}_{32} \mathbf{A}_{22}^{-1} \mathbf{A}_{23} - \mathbf{A}_{34} \mathbf{A}_{44}^{-1} \mathbf{A}_{43},$$

$$(13) \quad \mathbf{T}_{35} = \mathbf{A}_{35} - \mathbf{A}_{34} \mathbf{A}_{44}^{-1} \mathbf{A}_{23},$$

and so on. The reduced right-hand sides  $\tilde{\mathbf{f}}$  are defined as

$$(14) \quad \tilde{\mathbf{f}}_1 = \mathbf{f}_1 - \mathbf{A}_{12} \mathbf{A}_{22}^{-1} \mathbf{f}_2,$$

$$(15) \quad \tilde{\mathbf{f}}_3 = \mathbf{f}_3 - \mathbf{A}_{32} \mathbf{A}_{22}^{-1} \mathbf{f}_2 - \mathbf{A}_{34} \mathbf{A}_{44}^{-1} \mathbf{f}_4,$$

$$(16) \quad \tilde{\mathbf{f}}_5 = \mathbf{f}_5 - \mathbf{A}_{54} \mathbf{A}_{44}^{-1} \mathbf{f}_4 - \mathbf{A}_{56} \mathbf{A}_{66}^{-1} \mathbf{f}_6,$$

etc.

**3.2. Rank structure in the reduced blocks.** We next discuss algebraic properties of the blocks of the reduced coefficient matrix that allow for  $\mathbf{T}$  to be formed efficiently. The sub-blocks of  $\mathbf{T}$  are Schur-complements of sparse matrices. For instance, block  $\mathbf{T}_{11}$  has the formula

$$(17) \quad \mathbf{T}_{11} = \mathbf{A}_{11} - \mathbf{A}_{12} \mathbf{A}_{22}^{-1} \mathbf{A}_{21},$$

where  $\mathbf{A}_{11}, \mathbf{A}_{12}, \mathbf{A}_{21}$  are sparse with  $\mathcal{O}(n_2)$  non-zero entries and  $\mathbf{A}_{22}$  is a sparse banded matrix. Factorizing  $\mathbf{A}_{22}$  can be done efficiently using a sparse direct solver, but forming  $\mathbf{A}_{22}^{-1} \mathbf{A}_{21}$  naively may be slow and memory-intensive, especially considering that  $\mathbf{A}_{21}$  is sparse and would need to be converted to dense to interface with solve routines.

We use an alternate approach for efficiently forming  $\mathbf{T}_{11}$  that achieves high arithmetic intensity while maintaining a very low memory footprint. First, we prove algebraic properties about  $\mathbf{T}_{11}$ , which is a dense but structured matrix that only needs  $\mathcal{O}(n_2 b)$  storage in exact precision. The matrix  $\mathbf{T}_{11}$  is compressible in a format called Hierarchically Block-Separable (HBS) or Hierarchically Semi-Separable (HSS) with exact HBS rank at most  $2b$ . HBS matrices are a type of hierarchical matrix ( $\mathcal{H}^2$ -matrix), which allow dense matrices to be stored efficiently by

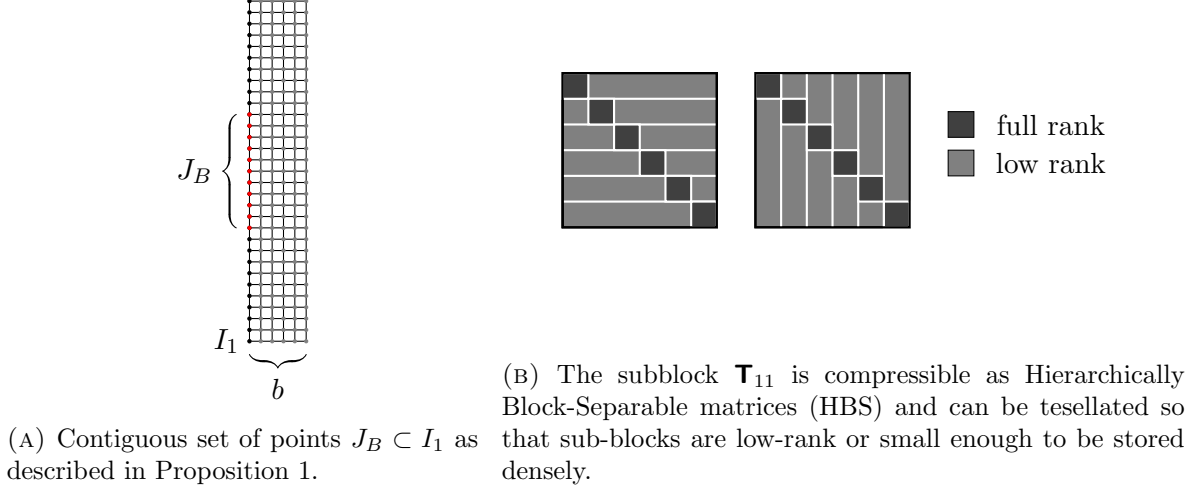


FIGURE 5. The geometry of slab interface  $I_1$  is shown in Figure 5a. The sub-matrix  $\mathbf{T}_{11}$  is compressible as an HBS matrix (cf. Figure 5b for an illustration).

exploiting low-rank structure in sub-blocks at different levels of granularity [10, 42, 52]. The sub-blocks of  $\mathbf{T}$  are also compressible in  $\mathcal{H}$ -matrix formats, e.g. Hierarchical Off-Diagonal Low Rank (HODLR). The rank property of  $\mathbf{T}_{11}$  is formally stated in Proposition 1.

After establishing the HBS structure of  $\mathbf{T}_{11}$ , we then describe how this structure can be recovered with only  $\mathcal{O}(b)$  matrix vector products of  $\mathbf{T}_{11}$  and  $\mathbf{T}_{11}^*$ . Vectors can efficiently be applied because  $\mathbf{T}_{11}$  and its transpose are compositions of sparse matrices. Since  $\mathbf{T}_{11}$  is admissible as a HODLR matrix, the structure can be efficiently recovered from matrix-vector products in this format as well [49, 51], though more vectors are required for reconstruction in this format.

**Proposition 1** (Rank Property). *Let  $J_B$  be a contiguous set of points on the slab interface  $I_1$ , and let  $J_F$  be the rest of the points  $J_F = I_1 \setminus J_B$ . The sub-matrices  $(\mathbf{T}_{11})_{BF}$ ,  $(\mathbf{T}_{11})_{FB}$  of the matrix  $\mathbf{T}$  have exact rank at most  $2b$ .*

See Figure 5 for an illustration of the slab interface and the resulting structure the sub-blocks of  $\mathbf{T}$ , which are defined in (9-13). The proof is in Appendix A.

**3.3. Recovering  $\mathcal{H}^2$ -matrix structure from matrix-vector products.** We next describe how to extract an  $\mathcal{H}^2$ -matrix representation of the reduced blocks purely from matrix-vector products. For concreteness, we are trying to recover  $\mathbf{T}_{11} \in \mathbb{R}^{n_2 \times n_2}$  as an HBS matrix with HBS rank at most  $2b$ . Typically,  $\mathcal{H}^2$ -matrices are used when the cost of forming or factorizing these matrices densely, is prohibitively large. In the context of SlabLU,  $\mathbf{T}_{11} \in \mathbb{R}^{n_2 \times n_2}$  can be stored densely for the problem sizes of interest, but traditional methods for forming  $\mathbf{T}_{11}$  densely may be inefficient, as described in Section 3.2. Instead, we recover  $\mathbf{T}_{11}$  as an HBS matrix with HBS rank at most  $2b$  from matrix-matrix products

$$(18) \quad \mathbf{Y}_{n_2 \times s} = \mathbf{T}_{11} \mathbf{\Omega}_{n_2 \times s}, \quad \mathbf{Z}_{n_2 \times s} = \mathbf{T}_{11}^* \mathbf{\Psi}_{n_2 \times s},$$

where  $\mathbf{\Omega}, \mathbf{\Psi}$  are Gaussian random matrices and  $s = 6b$  using the algorithm presented in [45]. This is theoretically possible because an HBS matrix of size  $n_2 \times n_2$  with HBS rank at most  $2b$  can be encoded in  $\mathcal{O}(n_2 b)$  storage. The HBS structure can be recovered from samples  $\mathbf{Y}, \mathbf{Z}$  after post-processing in  $\mathcal{O}(n_2 b^2)$  flops. The algorithm presented in [45] can be seen as an extension of algorithms for recovering low-rank factors from random sketches [53]. A

particular advantage of these algorithms is that they scale linearly and are truly black-box. The matrix-matrix products (18) are simple to evaluate using the matrix-free formula (17) of  $\mathbf{T}_{11}$  and its transpose. Applying  $\mathbf{T}_{11}$  involves two applications of sparse matrices and two triangular solves using pre-computed sparse triangular factors.

#### 4. STAGE TWO: FACTORIZING THE REDUCED BLOCK TRIDIAGONAL COEFFICIENT MATRIX

The elimination of nodes interior to each slab that we described in Section 3 results in a reduced linear system

$$(19) \quad \mathbf{T}\tilde{\mathbf{u}} = \tilde{\mathbf{f}},$$

where  $\tilde{\mathbf{u}}$  is the reduced solution vector and where  $\tilde{\mathbf{f}}$  is the equivalent body load on slab interfaces  $I_1, I_3, \dots$ . The elimination process described in Section 3 results a block-tridiagonal reduced system (19) with sub-blocks that are compressible in HBS format. Solving a system involving a block tridiagonal matrix is straight-forward using a blocked version of Gaussian elimination, described in Algorithms 1 and 2.

**Algorithm 1:** Sweeping build stage.

Given a block-tridiagonal matrix  $\mathbf{T}$ , Algorithm 1 builds a direct solver for  $\mathbf{T}$ , with the result stored in the matrices  $\mathbf{S}_1, \mathbf{S}_3, \dots$

```

1  $\mathbf{S}_1 \leftarrow \mathbf{T}_{11};$ 
2 Compute and store  $\mathbf{S}_1^{-1}$ ;
3 for  $j = 2, \dots, n_1/b$  do
4    $\mathbf{S}_{2j+1} \leftarrow \mathbf{T}_{2j+1,2j+1} - \mathbf{T}_{2j+1,2j-1}\mathbf{S}_{2j-1}^{-1}\mathbf{T}_{2j-1,2j+1};$ 
5   Compute and store  $\mathbf{S}_{2j+1}^{-1};$ 

```

**Algorithm 2:** Sweeping solve.

Given a body load  $\tilde{\mathbf{f}}$  and precomputed inverses of  $\mathbf{S}_1, \mathbf{S}_3, \dots$ , Algorithm 2 computes the solution vector  $\tilde{\mathbf{u}}$  by overwriting the original vector in place.

```

1 for  $j = 1, \dots, n_1/b$  do
2    $\tilde{\mathbf{f}}_{2j+1} \leftarrow \tilde{\mathbf{f}}_{2j+1} - \mathbf{T}_{2j+1,2j-1}\mathbf{S}_{2j-1}^{-1}\tilde{\mathbf{f}}_{2j-1};$ 
3 for  $j = 1, \dots, n_1/b + 1$  do
4    $\tilde{\mathbf{f}}_{2j-1} \leftarrow \mathbf{S}_{2j-1}^{-1}\tilde{\mathbf{f}}_{2j-1};$ 
5 for  $j = n_1/b, \dots, 1$  do
6    $\tilde{\mathbf{f}}_{2j-1} \leftarrow \tilde{\mathbf{f}}_{2j-1} - \mathbf{S}_{2j-1}^{-1}\mathbf{T}_{2j-1,2j+1}\tilde{\mathbf{f}}_{2j+1};$ 
7  $\tilde{\mathbf{u}} \leftarrow \tilde{\mathbf{f}};$ 

```

The most elegant way to solve (19) is to compress the matrices  $\mathbf{S}_1, \mathbf{S}_3, \dots$  of Algorithm 1 as HBS using randomized black-box algorithms; this would lead to a solver with linear complexity in the case where the PDE is kept fixed as  $N$  increases. However, we have found that for two dimensional problems up to size  $N \approx 10^8$ , the sizes of the slab interfaces are small enough that dense linear algebra is the most efficient way to solve (19) in practice. After forming the sub-blocks of  $\mathbf{T}$  as HBS, we convert them to dense matrices as needed in Algorithm 1. We have observed that retaining HBS structure in the off-diagonal blocks of  $\mathbf{T}$  (as opposed to storing them densely) is useful to lower the memory footprint of the factorization and facilitate fast data movement from the CPU to the GPU in the implementation of Algorithm 1.

**Remark 2.** For Helmholtz problems of the form (2), we are often interested in evaluating the performance of a solver where the number of points per wavelength is fixed as  $N$  increases. In this regime, it is still possible to exploit rank structure in the blocks of  $\mathbf{T}$ ; however, the ranks will grow during the execution of Algorithm 1. To minimize rank-growth, an odd-even elimination order can be used instead of the sequential one in Algorithm 1 to keep the slabs as thin as possible during the factorization process. Due to the substantial rank growth of oscillatory problems in this regime, the HBS algebra is not likely to perform better than highly-tuned dense linear algebra routines on the GPU. Factorizing  $\mathbf{S}_1, \mathbf{S}_3, \dots$  of Algorithm 1 using dense linear algebra allows us to side-step this complication and still achieve excellent performance in Section 6.3, as our method relies on the sparsity pattern of the original matrix only and leverages efficient GPU offloading.

## 5. ALGORITHM AND COMPLEXITY COSTS

In this section, we provide a summary of the proposed algorithm and discuss its complexity costs. We also analyze the complexity costs, and choose the buffer size  $b$  as a function of the number of grid points  $N = n_1 n_2$ , in order to balance costs and achieve competitive complexities for the build and solve times.

We briefly summarize the algorithm for SlabLU. In Stage One, we compute factorizations of the form

$$(20) \quad \begin{matrix} \mathbf{A}_{22}^{-1} & , & \mathbf{A}_{44}^{-1} & , \dots \\ n_2 b \times n_2 b & & n_2 b \times n_2 b & \end{matrix}$$

for  $n_1/b$  sparse matrices. The reduced matrix  $\mathbf{T}$  is constructed using efficient black-box algorithms that recover  $\mathbf{T}_{11}, \mathbf{T}_{13}, \mathbf{T}_{31}, \mathbf{T}_{33}, \dots$  in HBS format through a random sampling method, as discussed in Section 3.3. It is important to note that Stage One can be trivially parallelized for each slab.

In Stage Two, the reduced system  $\mathbf{T}$  is factorized. Because the sub-blocks of  $\mathbf{T}$  are HBS, this structure can be used to create a linear solver. However, we have found empirically that for 2D problems, the blocks are small enough that using dense linear algebra is just as fast, and much easier to implement. The simplified scheme using dense matrix algebra has an additional benefit in that it relies on sparsity alone; this makes it well suited for highly oscillatory problems, as it is immune to the rank-growth that typically happens when the wavenumber  $\kappa$  grows with  $N$ , cf. Remark 2.

**Algorithm 3:** Factorizing  $\mathbf{A}$  using SlabLU.

- 1 **for**  $j=1, \dots, n_1/b$  **do**
- 2   | Compute  $\mathbf{A}_{2j,2j}^{-1}$  using black-box sparse direct solvers.
- 3   | Compress  $\mathbf{T}_{11}, \mathbf{T}_{13}, \dots$  as HBS matrices with randomized black-box compression using matrix-free formulas, e.g. (17).
- 4   | Factorize  $\mathbf{T}$  using Algorithm 1.

**Algorithm 4:** Solving  $\mathbf{A}\mathbf{u} = \mathbf{f}$  using SlabLU.

- 1 Calculate the equivalent body  $\tilde{\mathbf{f}}$  on  $I_1, I_3, \dots$  using (14-16) in parallel.  
    // Parallel computation
- 2 Solve  $\mathbf{T}\tilde{\mathbf{u}} = \tilde{\mathbf{f}}$  for  $\tilde{\mathbf{u}}$  on  $I_1, I_3, \dots$  using Algorithm 2.  
    // Serial algorithm
- 3 Solve for  $\mathbf{u}$  on  $I_2, I_4, \dots$  using  $\tilde{\mathbf{u}}$  on  $I_1, I_3, \dots$  with (7) in parallel.  
    // Parallel computation

**5.1. Algorithmic complexity.** When rank-structure is exploited in both Stage One and Stage Two, choosing the slab width  $b = \mathcal{O}(1)$  leads to overall linear complexity (in the case where the equation is kept fixed as  $N$  is increased). In the simplified scheme relying on dense linear algebra in the second stage, we can choose the buffer size to balance the costs of the two stages. We first demonstrate how to choose  $b$  for the 2nd order finite difference stencil, then repeat the process for the HPS discretization. The asymptotic costs with  $N$  are the same for both discretizations, and as described in Section 5.3; there are pre-factors that depend on the local polynomial order  $p$  for the HPS discretization. For both discretizations we report  $T_{\text{build}}$ , which is the asymptotic flop cost to build the direct solver and  $M$  which is the memory in bits required to store the direct solver. The flop cost to apply the direct solver is  $T_{\text{solve}}$  and is the same asymptotically as  $M$  unless otherwise mentioned.

**5.2. Complexity analysis for 2nd order finite difference discretization.** Stage One requires computing sparse factorizations (20) for each thin slab, then constructing the sub-blocks of  $\mathbf{T}$  in HBS format using a randomized black-box algorithm. For each slab, the local sparse matrix is of size  $n_2 b \times n_2 b$  with bandwidth  $b$ ; the sparse factorization requires  $\mathcal{O}(n_2 b^3)$  flops to compute and  $\mathcal{O}(n_2 b^2)$  bits to store. Each sub-block of the reduced system  $\mathbf{T}$  is constructed as an HBS matrix using a randomized sampling algorithm, for which the dominant cost is constructing the random samples (18), which requires  $\mathcal{O}(n_2 b^3)$  flops using matrix-free formulas for applying (cf. equation (17) for the formula to apply  $\mathbf{T}_{11}$ ).

Stage Two involves a factorization of  $\mathbf{T}$  using Algorithm 1. For generality, consider that  $T_{\mathbf{S}}$  and  $M_{\mathbf{S}}$  are the time and memory, respectively needed for the factorization of each matrix  $\mathbf{S}_1, \mathbf{S}_3, \dots$  of size  $n_2 \times n_2$ . Then the total costs of computing and storing SlabLU are

$$(21) \quad \begin{aligned} T_{\text{build}} &= \mathcal{O}\left(\frac{n_1}{b} n_2 b^3\right) + \mathcal{O}\left(\frac{n_1}{b} T_{\mathbf{S}}\right), & M &= \mathcal{O}\left(\frac{n_1}{b} n_2 b^2\right) + \mathcal{O}\left(\frac{n_1}{b} M_{\mathbf{S}}\right). \\ &\text{sparse slab} & &\text{sparse slab} \\ &\text{factorizations} & &\text{factorizations} \end{aligned}$$

Because direct solvers are typically limited by their memory costs, we choose  $b$  to minimize the memory footprint. This depends on the choice of matrix format used for the matrices  $\mathbf{S}_1, \mathbf{S}_3, \dots$ . For instance, the use of HBS algebra gives  $T_{\mathbf{S}} = \mathcal{O}(k n_2)$  and  $M_{\mathbf{S}} = \mathcal{O}(k^2 n_2)$ . When the PDE is fixed as  $N$  grows, the resulting complexity is

$$(22) \quad b = \mathcal{O}(\sqrt{k}) \quad \Rightarrow \quad T_{\text{build}} = \mathcal{O}(k^{1.5} N), \quad M = \mathcal{O}(k^{0.5} N)$$

The use of dense linear algebra to factorize  $\mathbf{T}$  gives

$$(23) \quad b = \mathcal{O}(\sqrt{n_2}) \quad \Rightarrow \quad T_{\text{build}} = \mathcal{O}(n_1 n_2^{2.5}), \quad M = \mathcal{O}(n_1 n_2^{1.5}),$$

which scales particularly well for domains with high aspect ratio when  $n_1 > n_2$ . SlabLU provides a flexible framework for choosing  $b$  depending on the choice of rank-structured linear algebra in factorizing  $\mathbf{T}$ . Likewise, the buffer size  $b$  can be chosen for block low-rank formats [3]. The convenience of SlabLU lies in the fact that the matrices  $\mathbf{S}_1, \mathbf{S}_3, \dots$  are roughly the same size, and the  $\mathcal{H}$  or  $\mathcal{H}^2$  algebra is much simpler to optimize for performance.

In our numerical results, we used dense linear algebra to factorize  $\mathbf{T}$ , which is highly effective and robust for oscillatory problems in 2D, up to  $N \approx 10^8$ . Section 6 features a variety of rectangular and curved domains, as well as square domains, which is the adversarial worst case in terms of the algorithm complexity in (23). When  $n_1 = n_2$ , the complexity is  $T_{\text{build}} = \mathcal{O}(N^{1.75})$  and  $M = \mathcal{O}(N^{1.25})$ , though complexities observed in Section 6 for  $T_{\text{build}}$  are practically linear, especially when using GPU off-loading.

**5.3. Complexity analysis for HPS discretization.** The numerical results feature a high order discretization scheme that interfaces particularly well with sparse direct solvers which we use to resolve high frequency scattering problems to high accuracy. As discussed in Section 2.3, HPS is a spectral collocation discretization that employs multiple subdomains to enforce

the PDE using spectral differentiation. The subdomains are coupled together by ensuring continuity of the solution and its derivative across subdomains.

A natural approach to factorizing the sparse coefficient matrix is to first factorize each leaf subdomain in parallel with  $\mathcal{O}(p^4N)$  flops, cf. Figure 3 for a description of static condensation. Then, the remaining sparse matrix  $\tilde{\mathbf{A}}$  of size roughly  $N/p \times N/p$  is factorized using SlabLU. Because  $\tilde{\mathbf{A}}$  is smaller, the costs of factorizing  $\tilde{\mathbf{A}}$  with SlabLU involves prefactors with  $p$ . In particular, the sparse factorization of a thin slab of width  $b$  requires  $\mathcal{O}\left(\frac{n_2}{\sqrt{p}}b^3\right)$  flops to compute and  $\mathcal{O}\left(\frac{n_2}{\sqrt{p}}b^2\right)$  bits to store. As we did in equation (21), we can choose  $b$  to minimize the memory cost of storing the factorization of  $\tilde{\mathbf{A}}$ , leading to prefactors of  $\sim 1/\sqrt{p}$  in equations (22, 23).

Traditionally, the pre-factor cost of static condensation has been considered prohibitively expensive. However, [69] describes simple GPU optimizations that use batched linear algebra to significantly accelerate these operations; they are so efficient that we can save on storage costs by not explicitly storing the factorizations of the local spectral differentiation matrices in each HPS subdomain. Instead, we can reform and refactor these matrices as needed, leading to a decreased cost in storage (only the factorization of  $\tilde{\mathbf{A}}$  is stored) and an increased cost in applying the factorization of  $\mathbf{A}$ .

## 6. NUMERICAL EXPERIMENTS

In this section, we demonstrate the effectiveness of our solver through a series of numerical experiments. We report the build time, solve time, and accuracy of solving constant and variable-coefficient elliptic PDEs using two collocation-based discretization schemes on both rectangular and curved geometries. Our experiments were conducted on various hardware architectures to showcase the portability and ease of performance tuning of our framework. We utilize a high-order multidomain spectral collocation scheme, briefly introduced in Section 2.3, to solve challenging scattering phenomena. The high-order discretization scheme allows us to accurately discretize the PDE, while the flexibility of the multidomain scheme enables us to solve PDEs on curved domains using SlabLU. The combination of SlabLU and high-order discretization provides a powerful tool for simulating electromagnetic and acoustic scattering.

We have implemented SlabLU in an open-source software package, `slabLU`, in Python [68]. It is designed to be efficient and portable across various hardware architectures. The source code, detailed documentation, and usage examples are provided to facilitate the reproduction of our numerical results. We conducted the experiments on three different architectures: (1) a 16-core Intel i9-12900k CPU with 128 GB of RAM, (2) an NVIDIA RTX 3090 GPU with 24 GB of memory and access to 128 GB of RAM, and (3) an NVIDIA V100 with 32 GB of memory and access to 768 GB of RAM. We chose to run experiments on architectures (1) and (2) to demonstrate that the memory volume required to run SlabLU is reasonable. All experiments used double precision.

In our implementation, we use GPU offloading for Stage One and Stage Two in the factorization of  $\mathbf{A}$  using SlabLU, for architectures (2) and (3). In Stage One, we wrote custom sparse direct solvers for sparse systems (20) using GPU acceleration. This allowed us to achieve substantial acceleration in generating random sketches (18) of each subblock of  $\mathbf{T}$ . The implementation also uses batched linear algebra [1] to post-process sketches and recover the subblocks of  $\mathbf{T}$  as HBS matrices. In Stage Two, we use the HBS structure of  $\mathbf{T}$  to efficiently move the reduced system onto the GPU, then the matrices  $\mathbf{S}_1, \mathbf{S}_3, \dots$  of Algorithm 1 are factorized densely using highly optimized vendor libraries on the GPU. Recent works [2, 38] have demonstrated promising results in achieving high performance for sparse direct solvers on the GPU. Established library packages, such as STRUMPACK [37], have also incorporated GPU

support. The challenge in achieving optimal performance for such codes lies in careful load balancing and memory access patterns across a range of front sizes in a multi-level tree [44, 62]. SlabLU circumvents this difficulty using a two-level scheme that uses traditional sparse direct solvers for small fronts of size  $b$  and custom  $\mathcal{H}^2$ -matrix approaches for the larger fronts.

**6.1. Description of benchmark PDEs and accuracies reported.** We describe the PDEs used as benchmarks in our numerical experiments and how we calculate accuracy. We use the constant coefficient Helmholtz problem for various wavenumbers  $\kappa$

$$(24) \quad \begin{cases} -\Delta u(x) - \kappa^2 u(x) = 0, & x \in \Omega, \\ u(x) = u_{\text{true}}(x), & x \in \Gamma, \end{cases}$$

where the true solution  $u_{\text{true}} = J_0(\kappa\|x - (-0.1, 0.5)\|)$  and  $J_0$  is the zeroth Bessel function of the first kind.

After applying the direct solver, we obtain the calculated solution  $\mathbf{u}_{\text{calc}}$  at discretization points within the domain. We report the relative error with respect to the residual of the discretized system (3) and with respect to the true solution  $\mathbf{u}_{\text{true}}$  evaluated at the collocation points as follows:

$$(25) \quad \text{relerr}_{\text{res}} = \frac{\|\mathbf{A}\mathbf{u}_{\text{calc}} - \mathbf{f}\|_2}{\|\mathbf{f}\|_2}, \quad \text{relerr}_{\text{true}} = \frac{\|\mathbf{u}_{\text{calc}} - \mathbf{u}_{\text{true}}\|_2}{\|\mathbf{u}_{\text{true}}\|_2}.$$

We also report  $T_{\text{build}}$ , which is the wall-clock time needed to factorize the coefficient matrix  $\mathbf{A}$ , and  $M$ , which is the memory required to store the computed direct solver. Additionally, we report  $T_{\text{solve}}$  for one right-hand side vector, which is the time needed to apply the direct solver to solve systems (3), as described in Algorithm 4.

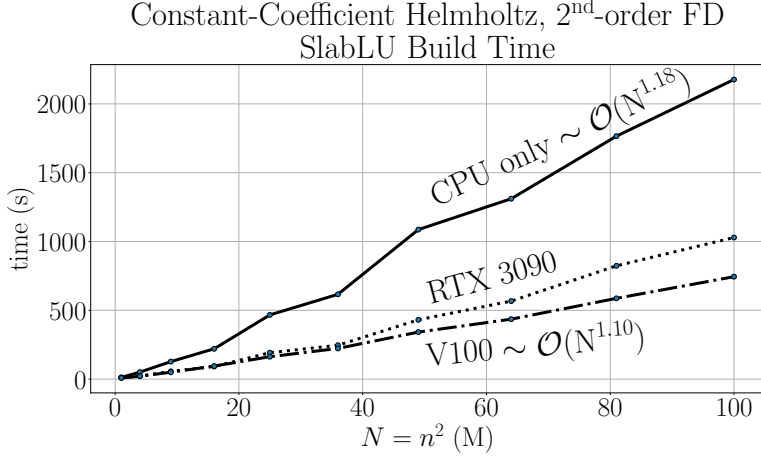
**6.2. Experiments using Low-Order Discretization.** In this section, we demonstrate how SlabLU performs on sparse coefficient matrices arising from PDEs discretized with 2nd order finite differences. We also compare SlabLU to SuperLU, a black-box sparse direct solver code.

We demonstrate competitive scaling for the build time of the factorization and for the memory footprint. See Figure 6 for the constant-coefficient Helmholtz equation (24). Despite the super-linear complexity scaling, the scaling appears to be linear for grids of size up to  $N = 100M$ . We discretize the Helmholtz equation to at least 10 points per wavelength to resolve the oscillatory solutions, leading to large grids. However, due to the effect of pollution when using low-order discretization, we need to discretize the Helmholtz equation to 250 points per wavelength to attain 3 digits of accuracy with respect to the known analytic solution.

We compare the performance of SlabLU and SuperLU in solving the 2nd order finite difference discretization of the constant coefficient Helmholtz equation (24), which results in very ill-conditioned sparse matrices (3) that need to be solved. SuperLU [13, 48] is a generic sparse direct solver that computes a sparse LU factorization of any given sparse matrix to high accuracy. We use the Scipy interface (version 1.8.1) to call SuperLU with the default permutation specification of COLAMD ordering; this version of SuperLU is sequential with multi-threading for BLAS calls.

The primary purpose of the comparison to this version of SuperLU is to compare accuracy of the computed factorization. Sparse direct solvers use sparsity in the discretized operator in order to factorize the sparse coefficient matrix exactly. SlabLU uses sparsity in the traditional sense for the sparse factorizations (20) in Stage One and approximately constructs the reduced system  $\mathbf{T}$  to high accuracy using randomized black-box sampling (cf. Section 3.3.) Both schemes are able to resolve the solution up to the discretization error (cf. Figure 7).

SlabLU also compares favorably to SuperLU in terms of memory costs; this is slightly surprising because the memory costs of SlabLU have slightly worse asymptotic scaling, compared

(A) Timing results for factorizing  $\mathbf{A}$  using SlabLU on various architectures.

$N$	$b$	$\kappa$	$M$	$T_{\text{solve}}$	$\text{relerr}_{\text{res}}$	$\text{relerr}_{\text{true}}$
1.0 M	50	27.1	0.5 GB	0.9 s	1.1e-11	1.8e-03
4.0 M	100	52.3	2.5 GB	2.9 s	1.8e-11	2.6e-03
9.0 M	125	77.4	6.6 GB	7.3 s	2.6e-11	4.0e-03
16.0 M	160	102.5	12.9 GB	10.4 s	2.4e-11	1.0e-02
25.0 M	200	127.7	22.5 GB	15.2 s	2.5e-11	1.0e-02
36.0 M	200	152.8	32.3 GB	21.7 s	2.8e-11	4.8e-03
49.0 M	200	177.9	46.9 GB	31.8 s	4.2e-11	6.5e-03
64.0 M	250	203.1	64.0 GB	42.8 s	1.4e-10	3.1e-02
81.0 M	250	228.2	83.8 GB	75.5 s	8.5e-11	1.1e-02
100.0 M	250	253.3	105.7 GB	88.6 s	6.7e-11	8.7e-03
			$\sim \mathcal{O}(N^{1.16})$	$\sim \mathcal{O}(N^{1.09})$		

(B) The table reports how  $b$  grows as a function of the problem size  $N$ , as well as  $M, T_{\text{solve}}$  and the computed relative accuracies. The wavenumber  $\kappa$  is increased with the problem size to maintain 250 points per wavelength. Though the solution is resolved to at least 10 digits in the residual, the relative error compared to the true solution is only 3 digits. For these experiments,  $T_{\text{solve}}$  is reported on the CPU architecture.

FIGURE 6. Helmholtz equation (eq. 24) discretized with 2nd order finite differences with constant points per wavelength.

to multi-level schemes. We believe may be because of inefficiencies of storing the sparse factorization or because COLAMD chooses a suboptimal ordering, compared to a METIS ordering, which is not available for this version. For problems larger than 10.2M points, SuperLU does not compute the factorization, because the memory requirements exceed some pre-prescribed limit. The authors note that more optimized solvers are available that use multi-threading or MPI parallelism [5, 17, 47]; comparison to these solvers will be the subject of future work.

**6.3. Solving challenging scattering problems with high order discretization.** High-order discretization is crucial for resolving variable-coefficient scattering phenomena due to the pollution effect, which requires increasing the number of points per wavelength as the domain size increases [11, 20]. The HPS discretization (cf. Section 2.3) is less sensitive to pollution because it allows for a high choice of local polynomial order [40, 50]. In Helmholtz experiments, HPS with  $p = 22$  accurately resolves oscillatory solutions using only 10 points per wavelength on domains up to size  $1000\lambda \times 1000\lambda$ , while 2nd order FD requires 100-250 points per wavelength to achieve low accuracy. Combining HPS with SlabLU provides a powerful tool for resolving challenging scattering phenomena to high accuracy, especially for situations where efficient preconditioners are not available [27]. We first demonstrate the

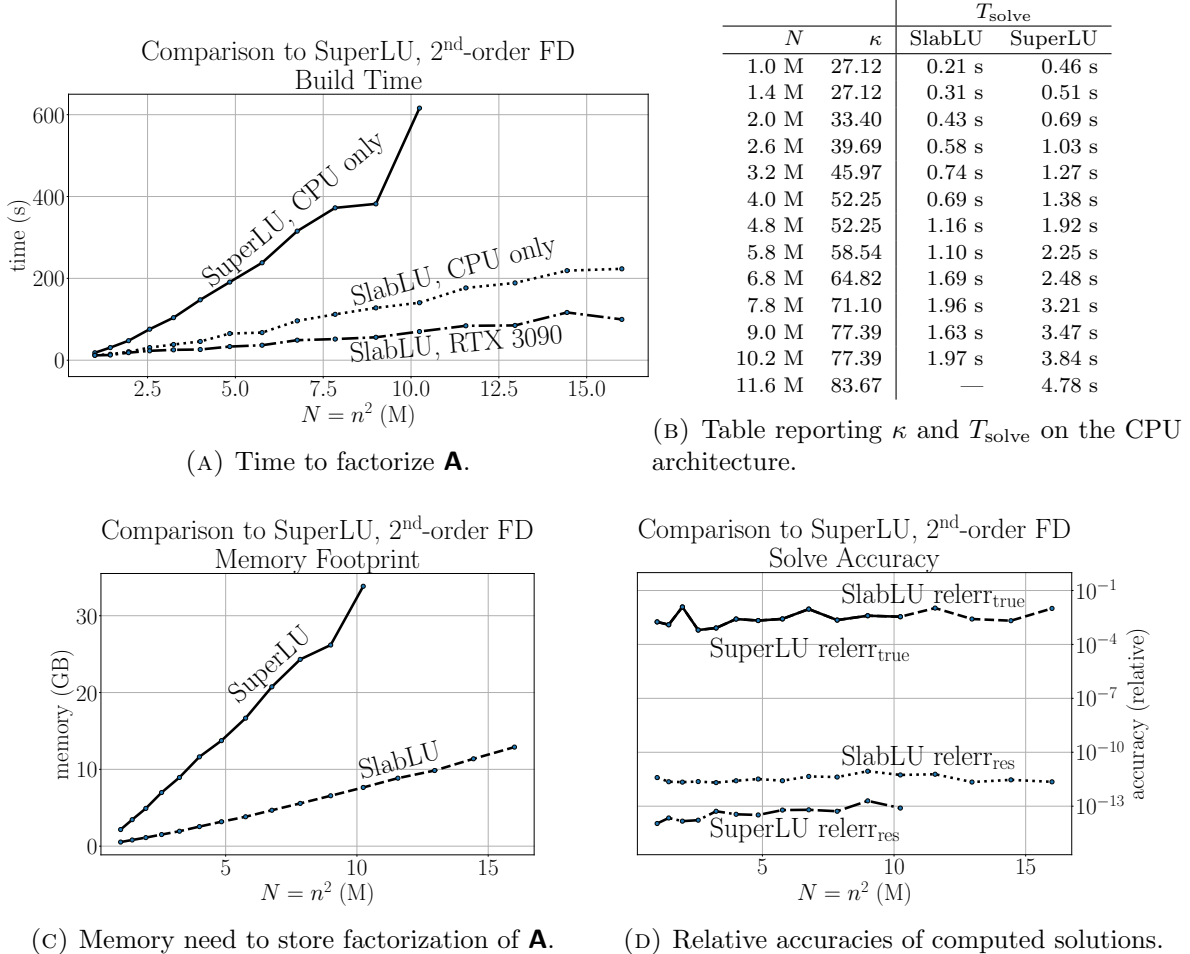
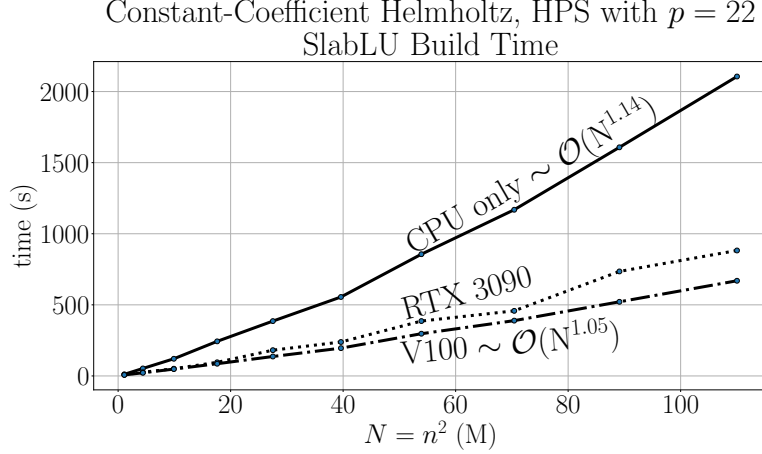


FIGURE 7. Comparison to a sequential version of Super LU for 2d order FD which uses multi-threading through BLAS calls. SlabLU uses approximations (cf. Algorithm 3) for construction of the reduced system  $\mathbf{T}$  and efficiently factorizes the system (3) to high accuracy. Our comparison shows that SlabLU outperforms this version of SuperLU in terms of build times and memory costs. For the CPU-comparison, SlabLU is faster by a factor of 4 for  $N=10.2\text{M}$ . Using GPU acceleration makes the method faster by a factor of 8. Additionally, SlabLU is more memory efficient by a factor of 4 for  $N = 10.2\text{M}$ .

performance of SlabLU for sparse coefficient matrices arising from the HPS discretization on a benchmark PDE of constant coefficient Helmholtz in Figure 8. As discussed in Section 5.3, the leaf operations are handled efficiently using batched linear algebra, and the local leaf factorizations are discarded and re-factorized as needed during the solve stage to save on memory costs for the direct solver.

We will now demonstrate the ability of HPS, combined with SlabLU as a sparse direct solver, to solve complex scattering phenomena on various 2D domains. For the presented PDEs, we will show how the accuracy of the calculated solution converges to a reference solution depending on the choice of  $p$  in the discretization. Specifically, we will solve the BVP (1) with the variable-coefficient Helmholtz operator (2) for Dirichlet data on curved and rectangular domains.

We fix the PDE and refine the mesh to compare calculated solutions to a reference solution obtained on a fine mesh with high  $p$ , as the exact solution is unknown. The relative error is

(A) Timing results for factorizing  $\mathbf{A}$  using SlabLU on various architectures.

$N$	$b$	$\kappa$	$M_{\text{build}}$	$T_{\text{solve}}$	relerr <sub>res</sub>	relerr <sub>true</sub>
1.1 M	100	630.3	0.3 GB	1.0 s	4.2e-12	2.4e-08
4.4 M	200	1258.6	1.8 GB	3.8 s	6.5e-12	9.5e-08
9.9 M	200	1886.9	4.4 GB	7.7 s	1.2e-11	2.2e-07
17.6 M	200	2515.3	8.9 GB	13.9 s	2.7e-11	4.0e-07
27.5 M	200	3143.6	15.6 GB	19.8 s	6.4e-11	9.4e-07
39.6 M	300	3771.9	21.5 GB	33.2 s	4.3e-10	7.3e-07
53.9 M	280	4400.2	32.3 GB	46.4 s	6.9e-11	7.9e-07
70.4 M	400	5028.5	45.8 GB	60.9 s	1.3e-09	5.0e-07
89.1 M	360	5656.9	61.0 GB	76.6 s	4.3e-10	1.2e-06
110.0 M	400	6285.2	80.0 GB	83.9 s	2.3e-10	7.5e-07
		$\sim \mathcal{O}(N^{1.17})$		$\sim \mathcal{O}(N^{1.00})$		

(B) The table reports how  $b$  grows as a function of the problem size  $N$ , as well as  $M_{\text{factor}}$ ,  $T_{\text{solve}}$  and the computed relative accuracies. The wavenumber  $\kappa$  is increased with the problem size to maintain 10 points per wavelength. Using a high order multidomain spectral collocation scheme allows us to avoid the effects of pollution and achieve at least 6 digits of relative accuracy, compared to the known solution. For these experiments,  $T_{\text{solve}}$  is reported on the NVIDIA V100 architecture.

FIGURE 8. Helmholtz equation (eq. 24) discretized with HPS discretization ( $p = 22$ ) with constant points per wavelength.

calculated by comparing  $\mathbf{u}_{\text{calc}}$  to the reference solution  $\mathbf{u}_{\text{ref}}$  at a small number of collocation points  $\{x_j\}_{j=1}^M$  using the  $l_2$  norm

$$(26) \quad \text{relerr}_{\text{approx}} = \frac{\|\mathbf{u}_{\text{calc}} - \mathbf{u}_{\text{ref}}\|_2}{\|\mathbf{u}_{\text{ref}}\|_2}.$$

We demonstrate the convergence on a unit square domain  $\Omega = [0, 1]^2$  with a variable coefficient field  $b_{\text{crystal}}$  corresponding to a photonic crystal, shown in Figure 9.

Next, we show the convergence on a curved domain  $\Psi$  with a constant-coefficient field  $b \equiv 1$ , where  $\Psi$  is a half-annulus given by an analytic parameterization over a reference rectangle. The domain  $\Psi$  is parametrized as

$$(27) \quad \Psi = \left\{ \left( \cos(\hat{\theta}(x_1)), \sin(\hat{\theta}(x_1)) \right) \text{ for } (x_1, x_2) \in [0, 3] \times [0, 1] \right\},$$

where  $\hat{\theta}(z) = \frac{\pi}{3}z$ . Using the chain rule, (2) on  $\Psi$  takes a different form of a variable-coefficient elliptic PDE on the reference rectangle. The solutions on  $\Psi$  and convergence plot are shown in Figure 10.

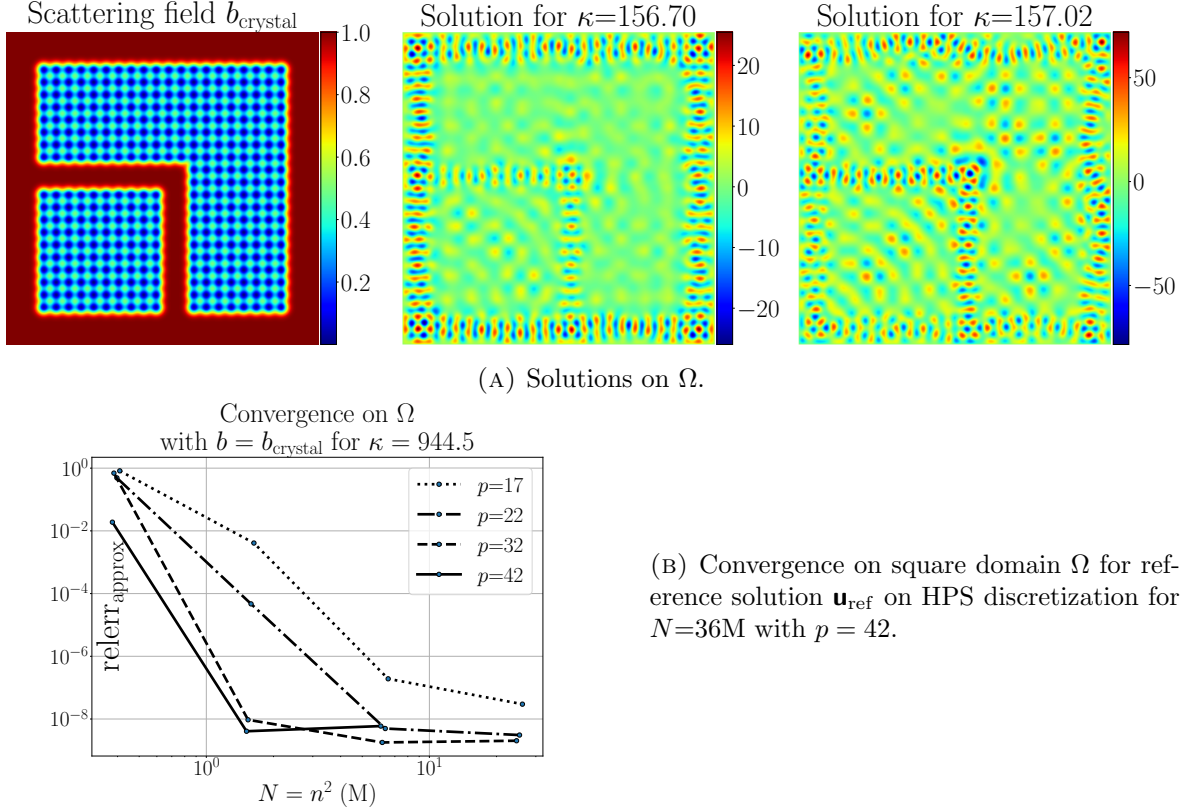


FIGURE 9. Solutions of variable-coefficient Helmholtz problem on domain  $\Omega$  with Dirichlet data  $u \equiv 1$  on  $\partial\Omega$  for various wavenumbers  $\kappa$ . The scattering field  $b_{\text{crystal}}$  is a photonic crystal with an extruded corner waveguide. The crystal is represented as a series of narrow Gaussian bumps with separation  $s = 0.04$  and is designed to filter wave frequencies that are roughly  $1/s$ .

Finally, we demonstrate convergence on a curved domain  $\Phi$  with a constant coefficient field  $b \equiv 1$ , where we have implemented a periodic boundary condition. The domain  $\Phi$  is parametrized by the formula

$$(28) \quad \Phi = \left\{ \left( \hat{r}(x_1, x_2) \cos(\hat{\theta}(x_1)), \hat{r}(x_1, x_2) \sin(\hat{\theta}(x_1)) \right) \text{ for } (x_1, x_2) \in [0, 6] \times [0, 1] \right\},$$

where  $\hat{r}(z_1, z_2) = 1 + \frac{1}{5} \cos\left(\frac{15}{\pi} z_1 + z_2\right)$  and  $\hat{\theta}(z) = \frac{\pi}{3} z$ . By applying the chain rule, the Helmholtz operator (2) on  $\Phi$  takes a different form of a variable-coefficient elliptic PDE on the reference rectangle. The solutions on  $\Phi$  and convergence plot are illustrated in Figure 11.

**Remark 3.** *When using large buffer sizes, the bound on the exact rank provided by Proposition 1 is often pessimistic. For non-oscillatory problems, the actual numerical rank is very modest, even when the buffer width  $b$  goes into the hundreds (cf. Table 8b). For oscillatory problems, a minimum of two points per wave-length is required, as measured at the thickest section of the slab, but the ranks are still far smaller than the strict bound of Prop 1.*

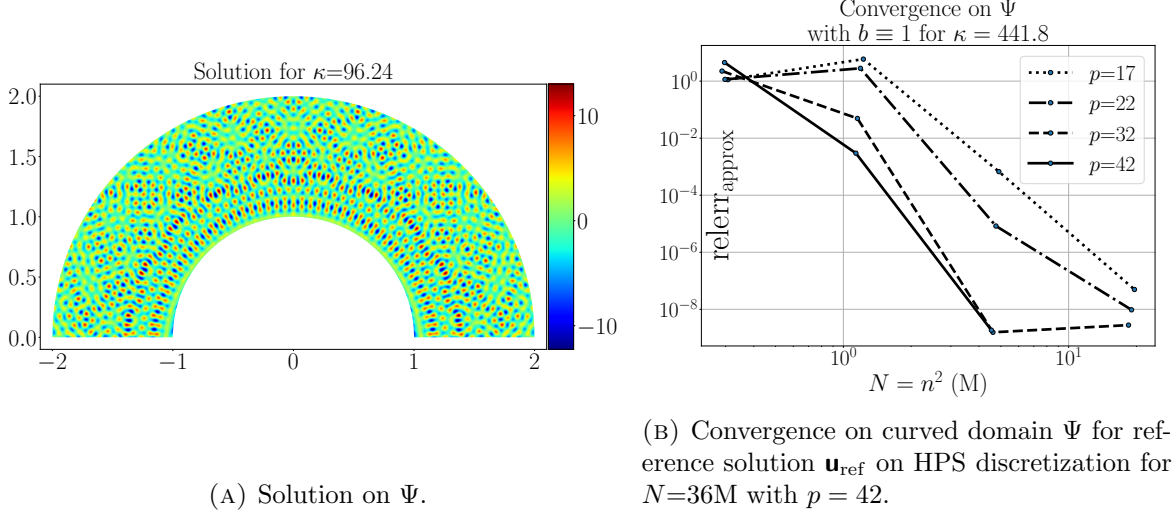


FIGURE 10. Solutions of constant-coefficient Helmholtz problem on curved domain  $\Psi$  with Dirichlet data given by  $u \equiv 1$  on  $\partial\Psi$ . The solutions are calculated parametrizing  $\Psi$  in terms of a reference rectangle domain as (27) and solving a variable-coefficient elliptic PDE on the reference rectangle.

## 7. CONCLUSION

This paper introduces SlabLU, a sparse direct solver framework designed for solving elliptic PDEs. The approach decomposes the domain into a sequence of thin slabs. The degrees of freedom internal to each slab are eliminated in parallel, yielding a reduced matrix  $\mathbf{T}$  defined on the slab interfaces. The reduced matrix  $\mathbf{T}$  has dense sub-blocks but is rich in  $\mathcal{H}$  and  $\mathcal{H}^2$  matrix structure which can be used in constructing a linear complexity direct solver for many elliptic PDEs.

One key innovation of the method is the use of randomized compression with a sparse direct solver to efficiently form  $\mathbf{T}$ . The dense sub-blocks of  $\mathbf{T}$  have exact rank deficiencies in the off-diagonal blocks present in both the non-oscillatory and oscillatory regimes. The use of randomized black-box algorithms provides a purely algebraic means of efficiently forming  $\mathbf{T}$  for a variety of PDE discretizations.

The numerical experiments presented in this paper demonstrate that SlabLU is highly effective when used in conjunction with high-order multi-domain spectral collocation schemes. The combination of SlabLU with high order discretization enables the rapid and accurate simulation of large-scale and challenging scattering phenomena on both rectangular and curved domains to high accuracy. The technique presented is algebraic and can readily be adapted to other standard discretization schemes such as finite element and finite volume methods that can be partitioned into slabs.

We are currently working to further accelerate SlabLU in two regards:

- (1) By maintaining a rank structured format for the blocks in the reduced coefficient matrix  $\mathbf{T}$ , the memory footprint of the scheme is reduced. Moreover, such a shift gives the scheme linear complexity in the regime where the PDE is kept fixed as  $N$  increases. (As opposed to the “fixed number of points per wavelength” scaling that is the gold standard for oscillatory problems.)
- (2) By replacing the sequential solve in the factorization of the reduced coefficient matrix  $\mathbf{T}$  by an odd-even ordering where every other block is eliminated in a hierarchical fashion, much higher parallelism can be attained.

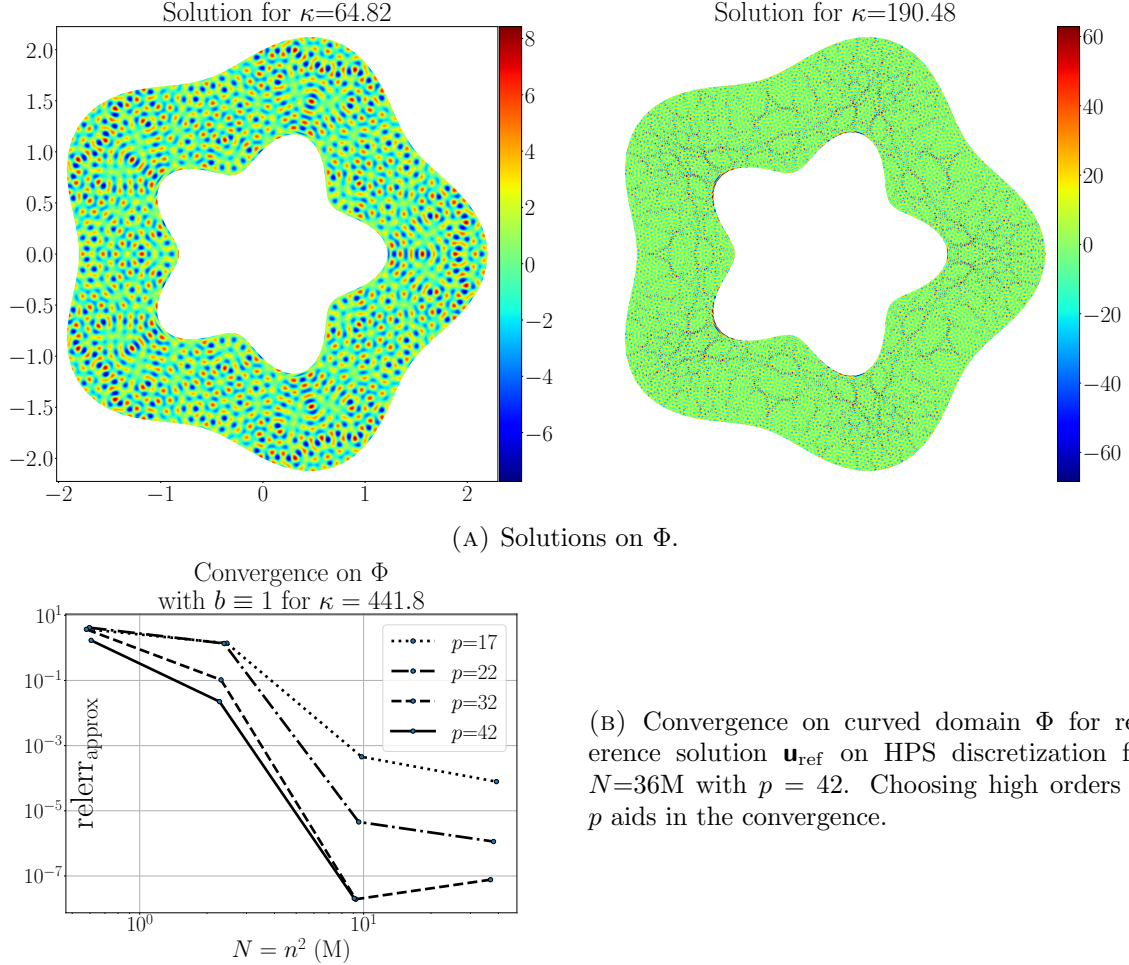


FIGURE 11. Solutions of constant-coefficient Helmholtz problem on curved domain  $\Phi$  with Dirichlet data  $u \equiv 1$  on  $\partial\Phi$  for various wavenumbers  $\kappa$ .

Both accelerations would in principle be helpful for 2D problems, but a key point of the current manuscript is that neither turned out to be necessary – very high efficiency and essentially linear scaling is maintained up to  $N \approx 10^8$  using GPU acceleration and dense linear algebra to factorize  $\mathbf{T}$ . In *three dimensions*, however, the situation is different. Here the blocks in the reduced coefficient matrix  $\mathbf{T}$  hold  $\sim N^{2/3}$  nodes, versus  $\sim N^{1/2}$  in 2D. This forces us to maintain the rank structured representations of these blocks throughout the computation, in part for purposes of computational speed, but primarily to keep storage requirements from becoming excessive. Recent work from the authors on the randomized black-box compression and factorization of  $\mathcal{H}^2$ -matrices with strong admissibility features useful algorithms and preliminary experiments for compressing the sub-blocks of  $\mathbf{T}$  for thin 3D slab domains [70]. The extension of SlabLU to 3D is in progress, and the work will be reported at a later time.

**Acknowledgements.** Anna would like to thank her dad, Andriy, for gifting her the RTX-3090 GPU. This version of the article has been accepted for publication, after peer review and is subject to Springer Nature’s AM terms of use, but is not the Version of Record and does not reflect post-acceptance improvements, or any corrections. The Version of Record is available online at: <https://doi.org/10.1007/s10444-024-10176-x>.

**Funding.** The work reported was supported by the Office of Naval Research (N00014-18-1-2354), by the National Science Foundation (DMS-2313434 and DMS-1952735), and by the Department of Energy ASCR (DE-SC0022251).

#### APPENDIX A. RANK PROPERTY OF THIN SLABS

In this appendix, we prove Proposition 1, which makes a claim on the rank structure of  $\mathbf{T}_{11}$ , defined in (17).

**Proposition 1** (Rank Property). *Let  $J_B$  be a contiguous set of points on the slab interface  $I_1$ , and let  $J_F$  be the rest of the points  $J_F = I_1 \setminus J_B$ . The sub-matrices  $(\mathbf{T}_{11})_{BF}$ ,  $(\mathbf{T}_{11})_{FB}$  of the matrix  $\mathbf{T}$  have exact rank at most  $2b$ .*

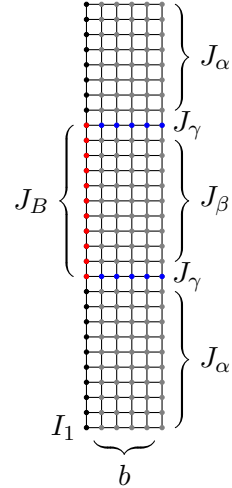


FIGURE 12. To assist in the proof of Proposition 1, we define a partitioning of the slab interface  $I_1 = J_B \cup J_F$ , where  $J_F = I_1 \setminus J_B$ . We also partition the slab interior nodes into  $I_2 := J_\alpha \cup J_\beta \cup J_\gamma$ .

Recall that  $\mathbf{T}_{11} = \mathbf{A}_{11} - \mathbf{A}_{12}\mathbf{A}_{22}^{-1}\mathbf{A}_{21}$ . The proof relies on the sparsity structure of the matrices in the Schur complement. As stated in the proposition, the slab interface  $I_1$  is partitioned into indices  $J_B$  and  $J_F$ . The proof relies on partitioning  $I_2$  as well, into the indices  $J_\alpha, J_\beta, J_\gamma$  shown in Figure 12, where  $|J_\gamma| = 2b$ .

The matrix  $\mathbf{A}_{22}$  is sparse and can be factorized as

$$(29) \quad \mathbf{A}_{22} = \mathbf{L}_{22}\mathbf{U}_{22} := \begin{bmatrix} \mathbf{L}_{\alpha\alpha} & & \\ & \mathbf{L}_{\beta\beta} & \\ \mathbf{L}_{\gamma\alpha} & \mathbf{L}_{\gamma\beta} & \mathbf{L}_{\gamma\gamma} \end{bmatrix} \begin{bmatrix} \mathbf{U}_{\alpha\alpha} & & \mathbf{U}_{\alpha\gamma} \\ & \mathbf{U}_{\beta\beta} & \mathbf{U}_{\beta\gamma} \\ & & \mathbf{U}_{\gamma\gamma} \end{bmatrix}$$

The formula for  $(\mathbf{T}_{11})_{FB}$  can be re-written as

$$(30) \quad (\mathbf{T}_{11})_{FB} = \mathbf{A}_{FB} - (\mathbf{A}_{F2}\mathbf{U}_{22}^{-1})(\mathbf{L}_{22}^{-1}\mathbf{A}_{2B}) := \mathbf{A}_{FB} - \mathbf{X}_{F2} \mathbf{Y}_{2B}$$

The factors  $\mathbf{X}_{F2}$  and  $\mathbf{Y}_{2B}$  have sparse structure, due the sparsity in the factorization (29) and the sparsity of  $\mathbf{A}_{F2}$  and  $\mathbf{A}_{2B}$ .

$$(31) \quad \mathbf{X}_{F2} = [\mathbf{A}_{F\alpha} \quad \mathbf{0} \quad \mathbf{A}_{F\gamma}] \mathbf{U}_{22}^{-1}, \quad \mathbf{Y}_{2B} = \mathbf{L}_{22}^{-1} \begin{bmatrix} \mathbf{0} \\ \mathbf{A}_{\beta B} \\ \mathbf{A}_{\gamma B} \end{bmatrix}$$

The factors  $\mathbf{X}_{F2}$  and  $\mathbf{Y}_{2B}$  have the same sparsity pattern as  $\mathbf{A}_{F2}$  and  $\mathbf{A}_{2B}$ , respectively. As a result,

$$(32) \quad (\mathbf{T}_{11})_{FB} = \mathbf{A}_{FB} - [\mathbf{X}_{F\alpha} \quad \mathbf{0} \quad \mathbf{X}_{F\gamma}] \begin{bmatrix} \mathbf{0} \\ \mathbf{Y}_{\beta B} \\ \mathbf{Y}_{\gamma B} \end{bmatrix} = \mathbf{A}_{F,B} \underset{\text{sparse, } \mathcal{O}(1) \text{ entries}}{=} - \mathbf{X}_{F\gamma} \mathbf{Y}_{\gamma B} \underset{\text{exact rank } 2b}{=} .$$

Similar reasoning can be used to show the result for  $(\mathbf{T}_{11})_{BF}$ .

## REFERENCES

- [1] Ahmad Abdelfattah, Timothy Costa, Jack Dongarra, Mark Gates, Azzam Haidar, Sven Hammarling, Nicholas J Higham, Jakub Kurzak, Piotr Luszczek, Stanimire Tomov, et al. A set of batched basic linear algebra subprograms and lapack routines. *ACM Transactions on Mathematical Software (TOMS)*, 47(3):1–23, 2021.
- [2] Ahmad Abdelfattah, Pieter Ghysels, Wajih Boukaram, Stanimire Tomov, Xiaoye Sherry Li, and Jack Dongarra. Addressing irregular patterns of matrix computations on GPUs and their impact on applications powered by sparse direct solvers. In *Proceedings of the International Conference on High Performance Computing, Networking, Storage and Analysis*, pages 1–14, 2022.
- [3] Patrick Amestoy, Alfredo Buttari, Jean-Yves l’Excellent, and Theo Mary. On the complexity of the block low-rank multifrontal factorization. *SIAM Journal on Scientific Computing*, 39(4):A1710–A1740, 2017.
- [4] Patrick R Amestoy, Timothy A Davis, and Iain S Duff. An approximate minimum degree ordering algorithm. *SIAM Journal on Matrix Analysis and Applications*, 17(4):886–905, 1996.
- [5] Patrick R Amestoy, Iain S Duff, Jean-Yves L’Excellent, and Jacko Koster. Mumps: a general purpose distributed memory sparse solver. In *International Workshop on Applied Parallel Computing*, pages 121–130. Springer, 2000.
- [6] Jared Lee Aurentz and Richard Mikaël Slevinsky. On symmetrizing the ultraspherical spectral method for self-adjoint problems. *Journal of Computational Physics*, 410:109383, 2020.
- [7] Tracy Babb, Adrianna Gillman, Sijia Hao, and Per-Gunnar Martinsson. An accelerated Poisson solver based on multidomain spectral discretization. *BIT Numerical Mathematics*, 58:851–879, 2018.
- [8] Lehel Banjai and Wolfgang Hackbusch. Hierarchical matrix techniques for low-and high-frequency helmholtz problems. *IMA journal of numerical analysis*, 28(1):46–79, 2008.
- [9] Natalie N Beams, Adrianna Gillman, and Russell J Hewett. A parallel shared-memory implementation of a high-order accurate solution technique for variable coefficient Helmholtz problems. *Computers & Mathematics with Applications*, 79(4):996–1011, 2020.
- [10] Mario Bebendorf. *Hierarchical matrices*, volume 63 of *Lecture Notes in Computational Science and Engineering*. Springer-Verlag, Berlin, 2008. A means to efficiently solve elliptic boundary value problems.
- [11] Hadrien Bériot, Albert Prinn, and Gwénaël Gabard. Efficient implementation of high-order finite elements for Helmholtz problems. *International Journal for Numerical Methods in Engineering*, 106(3):213–240, 2016.
- [12] Timo Betcke, Elwin van ’t Wout, and Pierre Gélat. Computationally efficient boundary element methods for high-frequency helmholtz problems in unbounded domains. *Modern Solvers for Helmholtz Problems*, pages 215–243, 2017.
- [13] Matthias Bollhöfer, Olaf Schenk, Radim Janalík, Steve Hamm, and Kiran Gullapalli. State-of-the-art sparse direct solvers. In *Parallel Algorithms in Computational Science and Engineering*, pages 3–33. Springer, New York NY, 2020.
- [14] Steffen Börm, Lars Grasedyck, and Wolfgang Hackbusch. Introduction to hierarchical matrices with applications. *Engineering analysis with boundary elements*, 27(5):405–422, 2003.
- [15] William L. Briggs, Van Emden Henson, and Steve F. McCormick. *A multigrid tutorial*. Society for Industrial and Applied Mathematics (SIAM), Philadelphia, PA, second edition, 2000.
- [16] Gustavo Chávez, George Turkiyyah, Stefano Zampini, Hatem Ltaief, and David Keyes. Accelerated cyclic reduction: A distributed-memory fast solver for structured linear systems. *Parallel Computing*, 74:65–83, 2018.
- [17] Timothy A Davis. Algorithm 832: Umfpack v4. 3—an unsymmetric-pattern multifrontal method. *ACM Transactions on Mathematical Software (TOMS)*, 30(2):196–199, 2004.
- [18] Timothy A Davis. *Direct methods for sparse linear systems*, volume 2. SIAM, Philadelphia PA, 2006.
- [19] Timothy A. Davis, Sivasankaran Rajamanickam, and Wissam M. Sid-Lakhdar. A survey of direct methods for sparse linear systems. *Acta Numerica*, 25:383 – 566, 2016.
- [20] Arnaud Deraemaeker, Ivo Babuška, and Philippe Bouillard. Dispersion and pollution of the FEM solution for the Helmholtz equation in one, two and three dimensions. *International journal for numerical methods in engineering*, 46(4):471–499, 1999.
- [21] I.S. Duff, A.M. Erisman, and J.K. Reid. *Direct Methods for Sparse Matrices*. Oxford, Oxford United Kingdom, 1989.
- [22] B. Engquist and L. Ying. Sweeping preconditioner for the Helmholtz equation: Hierarchical matrix representation. *Communications on Pure and Applied Mathematics*, 64(5):697–735, 2011.
- [23] Björn Engquist and Lexing Ying. Sweeping preconditioner for the Helmholtz equation: Moving perfectly matched layers. *Multiscale Modeling & Simulation*, 9(2):686–710, 2011.

- [24] Björn Engquist and Hongkai Zhao. Approximate separability of the green's function of the helmholtz equation in the high frequency limit. *Communications on Pure and Applied Mathematics*, 71(11):2220–2274, 2018.
- [25] Yogi A Erlangga, Cornelis Vuik, and Cornelis W Oosterlee. Comparison of multigrid and incomplete lu shifted-laplace preconditioners for the inhomogeneous helmholtz equation. *Applied numerical mathematics*, 56(5):648–666, 2006.
- [26] Yogi A Erlangga, Cornelis Vuik, and Cornelis Willebrordus Oosterlee. On a class of preconditioners for solving the helmholtz equation. *Applied Numerical Mathematics*, 50(3-4):409–425, 2004.
- [27] Oliver G Ernst and Martin J Gander. Why it is difficult to solve Helmholtz problems with classical iterative methods. *Numerical analysis of multiscale problems*, pages 325–363, 2012.
- [28] Daniel Fortunato. A high-order fast direct solver for surface pdes. *arXiv preprint arXiv:2210.00022*, 2022.
- [29] Daniel Fortunato, Nicholas Hale, and Alex Townsend. The ultraspherical spectral element method. *Journal of Computational Physics*, 436:110087, 2021.
- [30] Daniel Fortunato and Alex Townsend. Fast Poisson solvers for spectral methods. *IMA Journal of Numerical Analysis*, 40(3):1994–2018, 2020.
- [31] Martin J Gander, Laurence Halpern, and Frédéric Magoules. An optimized schwarz method with two-sided robin transmission conditions for the helmholtz equation. *International journal for numerical methods in fluids*, 55(2):163–175, 2007.
- [32] Martin J Gander and Hui Zhang. Restrictions on the use of sweeping type preconditioners for Helmholtz problems. In *International Conference on Domain Decomposition Methods*, pages 321–332. Springer, 2017.
- [33] Martin J Gander and Hui Zhang. A class of iterative solvers for the Helmholtz equation: Factorizations, sweeping preconditioners, source transfer, single layer potentials, polarized traces, and optimized schwarz methods. *Siam Review*, 61(1):3–76, 2019.
- [34] P. Geldermans and A. Gillman. An adaptive high order direct solution technique for elliptic boundary value problems. *SIAM Journal on Scientific Computing*, 41(1):A292–A315, 2019.
- [35] A. George. Nested dissection of a regular finite element mesh. *SIAM J. on Numerical Analysis*, 10:345–363, 1973.
- [36] P. Ghysels, X. Li, F. Rouet, S. Williams, and A. Napov. An Efficient Multicore Implementation of a Novel HSS-Structured Multifrontal Solver Using Randomized Sampling. *SIAM Journal on Scientific Computing*, 38(5):S358–S384, 2016.
- [37] Pieter Ghysels, Gustavo Chávez, Lucy Guo, Chris Gorman, Xiaoye S. Li, Yang Liu, Liza Rebrova, François-Henry Rouet, Theo Mary, and Jonas Actor. Strumpack.
- [38] Pieter Ghysels and Ryan Synk. High performance sparse multifrontal solvers on modern GPUs. *Parallel Computing*, 110:102897, 2022.
- [39] Adrianna Gillman, AlexH. Barnett, and Per-Gunnar Martinsson. A spectrally accurate direct solution technique for frequency-domain scattering problems with variable media. *BIT Numerical Mathematics*, 55(1):141–170, 2015.
- [40] Adrianna Gillman and Per-Gunnar Martinsson. A direct solver with  $O(N)$  complexity for variable coefficient elliptic PDEs discretized via a high-order composite spectral collocation method. *SIAM Journal on Scientific Computing*, 36(4):A2023–A2046, 2014.
- [41] Adrianna Gillman, Patrick Young, and Per-Gunnar Martinsson. A direct solver  $o(n)$  complexity for integral equations on one-dimensional domains. *Frontiers of Mathematics in China*, 7:217–247, 2012. 10.1007/s11464-012-0188-3.
- [42] Wolfgang Hackbusch. *Hierarchical matrices: algorithms and analysis*, volume 49. Springer, New York NY, 2015.
- [43] Sijia Hao and Per-Gunnar Martinsson. A direct solver for elliptic PDEs in three dimensions based on hierarchical merging of Poincaré–Steklov operators. *Journal of Computational and Applied Mathematics*, 308:419–434, 2016.
- [44] Kyungjoo Kim and Victor Eijkhout. Scheduling a parallel sparse direct solver to multiple gpus. In *2013 IEEE International Symposium on Parallel & Distributed Processing, Workshops and Phd Forum*, pages 1401–1408. IEEE, 2013.
- [45] James Levitt and Per-Gunnar Martinsson. Linear-Complexity Black-Box Randomized Compression of Hierarchically Block Separable Matrices. *arXiv preprint arXiv:2205.02990*, 2022.
- [46] James Levitt and Per-Gunnar Martinsson. Linear-complexity black-box randomized compression of rank-structured matrices. *SIAM Journal on Scientific Computing*, 46(3):A1747–A1763, 2024.
- [47] Xiaoye S Li and James W Demmel. Superlu\_dist: A scalable distributed-memory sparse direct solver for unsymmetric linear systems. *ACM Transactions on Mathematical Software (TOMS)*, 29(2):110–140, 2003.
- [48] Xiaoye S Li and Meiyue Shao. A supernodal approach to incomplete LU factorization with partial pivoting. *ACM Transactions on Mathematical Software (TOMS)*, 37(4):1–20, 2011.

- [49] L. Lin, J. Lu, and L. Ying. Fast construction of hierarchical matrix representation from matrix-vector multiplication. *Journal of Computational Physics*, 230(10):4071 – 4087, 2011.
- [50] Per-Gunnar Martinsson. A direct solver for variable coefficient elliptic PDEs discretized via a composite spectral collocation method. *Journal of Computational Physics*, 242:460–479, 2013.
- [51] Per-Gunnar Martinsson. Compressing rank-structured matrices via randomized sampling. *SIAM Journal on Scientific Computing*, 38(4):A1959–A1986, 2016.
- [52] Per-Gunnar Martinsson. *Fast direct solvers for elliptic PDEs*. SIAM, Philadelphia PA, 2019.
- [53] Per-Gunnar Martinsson and Joel A Tropp. Randomized numerical linear algebra: Foundations and algorithms. *Acta Numerica*, 29:403–572, 2020.
- [54] P.G. Martinsson. A fast randomized algorithm for computing a hierarchically semiseparable representation of a matrix. *SIAM Journal on Matrix Analysis and Applications*, 32(4):1251–1274, 2011.
- [55] P.G. Martinsson. A direct solver for variable coefficient elliptic pdes discretized via a composite spectral collocation method. *Journal of Computational Physics*, 242(0):460 – 479, 2013.
- [56] P.G. Martinsson and V. Rokhlin. A fast direct solver for scattering problems involving elongated structures. *Journal of Computational Physics*, 221:288–302, 2007.
- [57] E. Michielssen, A. Boag, and W. C. Chew. Scattering from elongated objects: direct solution in  $O(N \log^2 N)$  operations. *IEE Proc. Microw. Antennas Propag.*, 143(4):277 – 283, 1996.
- [58] S. Olver and A. Townsend. A fast and well-conditioned spectral method. *SIAM Review*, 55(3):462–489, 2013.
- [59] Grégoire Pichon, Eric Darve, Mathieu Faverge, Pierre Ramet, and Jean Roman. Sparse supernodal solver using block low-rank compression. In *2017 IEEE International Parallel and Distributed Processing Symposium Workshops (IPDPSW)*, pages 1138–1147. IEEE, 2017.
- [60] John W Ruge and Klaus Stüben. Algebraic multigrid. In *Multigrid methods*, pages 73–130. SIAM, Philadelphia PA, 1987.
- [61] Alexandre Vion, R Bélanger-Rioux, L Demanet, and Christophe Geuzaine. A DDM double sweep preconditioner for the Helmholtz equation with matrix probing of the DtN map. *Mathematical and Numerical Aspects of Wave Propagation WAVES*, 2013, 2013.
- [62] Richard Vuduc, Aparna Chandramowlishwaran, Jee Choi, Murat Guney, and Aashay Shringarpure. On the limits of GPU acceleration. In *Proceedings of the 2nd USENIX conference on Hot topics in parallelism*, volume 13, 2010.
- [63] Shen Wang, Maarten V. de Hoop, and Jianlin Xia. On 3d modeling of seismic wave propagation via a structured parallel multifrontal direct Helmholtz solver. *Geophysical Prospecting*, 59(5):857–873, 2011.
- [64] Shen Wang, Xiaoye S Li, Jianlin Xia, Yingchong Situ, and Maarten V De Hoop. Efficient scalable algorithms for solving dense linear systems with hierarchically semiseparable structures. *SIAM Journal on Scientific Computing*, 35(6):C519–C544, 2013.
- [65] J. Xia, S. Chandrasekaran, M. Gu, and X.S. Li. Fast algorithms for hierarchically semiseparable matrices. *Numerical Linear Algebra with Applications*, 17(6):953–976, 2010.
- [66] Jianlin Xia, Shivkumar Chandrasekaran, Ming Gu, and Xiaoye S. Li. Superfast multifrontal method for large structured linear systems of equations. *SIAM J. Matrix Anal. Appl.*, 31(3):1382–1411, 2010.
- [67] Jinchao Xu and Ludmil Zikatanov. Algebraic multigrid methods. *Acta Numerica*, 26:591–721, 2017.
- [68] Anna Yesypenko. Slablu: A two-level sparse direct solver for elliptic pdes in python, May 2024.
- [69] Anna Yesypenko and Per-Gunnar Martinsson. GPU optimizations for the Hierarchical Poincaré-Steklov Scheme. *arXiv preprint arXiv:2211.14969*, 2022.
- [70] Anna Yesypenko and Per-Gunnar Martinsson. Randomized strong recursive skeletonization: Simultaneous compression and factorization of  $\mathcal{H}$ -matrices in the black-box setting. *arXiv preprint arXiv:2311.01451*, 2023.